Theoretical and Applied Climatology (2024) 155:299–308
https://doi.org/10.1007/s00704-023-04634-7

RESEARCH

Effective climate sensitivity distributions from a 1D model of global ocean and land temperature trends, 1970–2021

Roy W. Spencer[1] · John R. Christy[1]

Received: 10 January 2023 / Accepted: 28 August 2023 / Published online: 16 September 2023

Abstract

Current theoretically based Earth system models (ESMs) produce Effective Climate Sensitivities (EffCS) that range over a factor of three, with 80% of those models producing stronger global warming trends for 1970–2021 than do observations. To make a more observationally based estimate of EffCS, a 1D time-dependent forcing-feedback model of temperature departures from energy equilibrium is used to match measured ranges of global-average surface and sub-surface land and ocean temperature trends during 1970–2021. In response to two different radiative forcing scenarios, a full range of three model free parameters are evaluated to produce fits to a range of observed surface temperature trends ($\pm 2\sigma$) from four different land datasets and three ocean datasets, as well as deep-ocean temperature trends and borehole-based trend retrievals over land. Land-derived EffCS are larger than over the ocean, and EffCS is lower using the newer Shared Socioeconomic Pathways (SSP245, 1.86 °C global EffCS, ± 34% range 1.48–2.15 °C) than the older Representative Concentration Pathway forcing (RCP6, 2.49 °C global average EffCS, ± 34% range 2.04–2.87 °C). The strongest dependence of the EffCS results is on the assumed radiative forcing dataset, underscoring the role of radiative forcing uncertainty in determining the sensitivity of the climate system to increasing greenhouse gas concentrations from observations alone. The results are consistent with previous observation-based studies that concluded EffCS during the observational period is on the low end of the range produced by current ESMs.

1 Introduction

The determination of the sensitivity of the climate system to increasing greenhouse gas concentrations, usually stated in terms of the surface temperature change in response to a doubling of pre-industrial levels of atmospheric CO_2 (2XCO2), has remained elusive. In the forcing-feedback paradigm of climate change departures from global energy balance, the top-of-atmosphere (TOA) radiative energy imbalance N is the sum of an imposed radiative forcing F and a feedback response -λΔT,

$$N = F - \lambda \Delta T, \tag{1}$$

where the net feedback factor λ determines the climate sensitivity and ΔT is the global average surface temperature departure from the normal equilibrium state (National Research Council 1979). For example, the radiative forcing from a doubling of atmospheric CO_2 is generally accepted to be 3.7 W m^{-2} (Forster et al. 2021) and as the system warms over many centuries, the TOA energy imbalance N is removed, and a final equilibrium climate sensitivity change in temperature ΔT is achieved at F/λ.

For over 30 years, the range of equilibrium climate sensitivities (ECS) diagnosed either from theory (3D Earth System Models, ESMs) or from observations has persisted over a broad range between 1.5 and 4.5 deg. C, with a few outlier estimates (Meehl et al. 2020, and references therein). The most recent estimates from ESMs participating in the sixth Coupled Model Intercomparison Project (CMIP6, Eyring et al. 2016) cover the widest range yet (1.8 to 5.7 deg. C) although the CMIP6 expert evaluation of the most likely range has narrowed to 2.5 to 4.0 deg. C, with a best estimate of 3.0 deg. C (IPCC 2021a). Due to the long time scale (centuries) required for the deep ocean to reach a new equilibrium state, the possibility that feedbacks can change on multi-century time scales, and the differences in efficacy of various forcing agents (e.g., aerosols vs. CO_2), a shorter-term "effective" climate sensitivity (EffCS, e.g., Gregory

✉ Roy W. Spencer
roy.spencer@nsstc.uah.edu

[1] Earth System Science Center, The University of Alabama in Huntsville, 320 Sparkman Drive, Huntsville, AL 35805, USA

et al. 2020) is usually preferred over ECS as a more practical measure for energy policy decisions and mitigation planning.

The EffCS uncertainty on a theoretical level arises from the complexity of the feedback responses of the climate system to a radiative imbalance, such as how clouds change to either amplify or dampen warming. On an observational basis, EffCS uncertainty comes from a lack of accurate knowledge of both the radiative forcing and the temperature response of the system to that forcing over the last 50 to 100 years or more. Gregory et al. (2020) addressed reasons why such estimates can produce biased results, for example due to the influence of major volcanic eruptions. Scafetta (2022) and references therein provide a range of generally low EffCS values diagnosed from the observational record.

Alternatively, one can instead examine shorter-term interannual co-variations between TOA radiative flux and temperature to estimate λ, but non-feedback variations in TOA radiative flux de-correlate those variations leading to underestimates of λ made through standard least-squares linear regression (e.g., Spencer and Braswell 2011). Additionally, uncertainty in diagnosing EffCS from observations arises from multi-decadal time scale internal fluctuations in the climate system which can cause 10–20 year periods with either strong warming or no warming unrelated to the system's long-term response to anthropogenic forcing (e.g., Meehl et al. 2013). Further complicating observational diagnosis of sensitivity are uncertain changes in the large heat storing capacity of the ocean which cause a delay in surface warming compared to if there was no sub-surface energy storage.

The diagnosis of EffCS from climate models is hindered by the tendency of ESMs to not conserve energy, either in the ocean or top-of-atmosphere, a feature which has persisted from CMIP3 (Spencer and Braswell 2014), CMIP5 (Hobbs et al. 2016), to CMIP6 (Irving et al. 2021). This is a fundamental concern since global warming is first and foremost an issue of energy conservation. While heat storage by the landmass is usually ignored in such evaluations, here we include an estimate of its impact on diagnosed climate sensitivity. Finally, we note that the global average surface warming since 1970 — the 50 + year period with the largest anthropogenic radiative forcing of the climate system — has been weaker in observations than in 80% of 36 CMIP6 climate models (Fig. 1).

The complexity of the wide range of processes which determine climate sensitivity, combined with the rather wide range of sensitivities exhibited by climate models, the non-closure of the energy budgets in those models, and the tendency for recent warming to be weaker in observations than in models, leads to a need for simple alternative methods for examining what range of sensitivities are implied by the observed rates of global warming. Since long-term warming represents the accumulation of heat energy in the climate

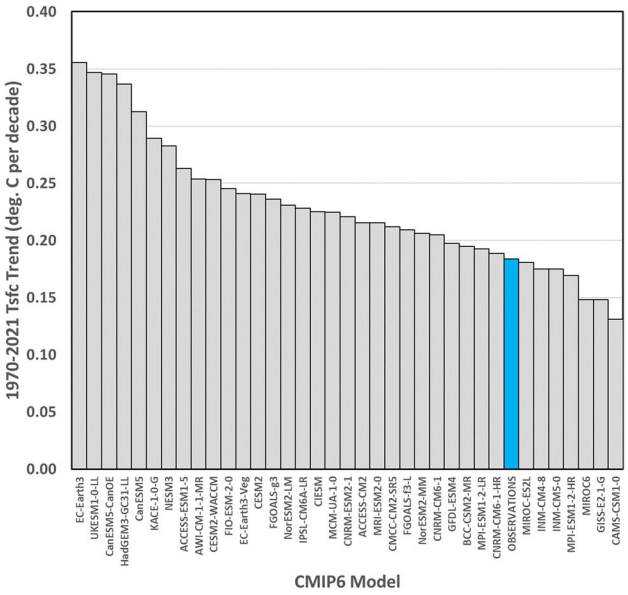

Fig. 1 Global average surface temperature trends in 36 CMIP6 models versus the average of four land and three ocean observational datasets (described in text) for the 52-year period 1970–2021

system resulting from a net top-of-atmosphere radiative energy imbalance, which in turn is the sum of an imposed radiative forcing and a climate feedback response to warming, it is straightforward to estimate the effective climate sensitivity during the observational record given estimates of warming and global radiative forcing using a 1D time-dependent model. Again, such an estimate is limited to the historical period, and how well it applies to future climate change is unknown.

The 1D result should not be expected to agree with the average of those ESM results since it has not yet been demonstrated that ESMs produce an unbiased distribution of warming trends (Fig. 1) and because of the tendency for models to not conserve energy during their time integration. Until the model state of the art reaches that point, it is useful to employ simple model frameworks that conserve energy, produce no model temperature drift, and can help answer the question, "What effective climate sensitivity is implied by observed rates of warming?".

Here we use a 1D time-dependent model of temperature departures from assumed energy equilibrium in 1765, over land and ocean separately, to diagnose EffCS for a range of observed temperature trends over land and ocean, utilizing two significantly different radiative forcing datasets (SSP245 and RCP6.0). The model could be considered the simplest approximation of ESMs where time-dependent equations are used to compute temperature tendencies in response to sources and sinks of energy. The simplicity of the model (1D rather than 3D, and only three ocean layers rather than up to 30) allows rapid computation of the sensitivity of EffCS

to choices of assumed TOA radiative forcing and temperature datasets. Here we include deep-ocean (below 2000 m) storage of heat as well as deep-land storage to 200 m depth, based upon borehole temperature measurements. The storage of heat in the global landmass is still not well handled by ESMs, which contain Land Surface Models (LSMs) with bottom boundary condition placement (BBCP) at only 2 to 10 m in depth (Cuesta-Valero et al. 2016; Burke et al. 2020; MacDougall et al. 2008, 2010), despite borehole evidence of warming to 200 m depth over recent centuries (National Research Council 2006; Harris and Chapman 2001).

The energy budget approach to estimating EffCS is similar to that of Lewis and Curry (2018), which obtained EffCS values ranging from 1.5 to 1.8 deg. C by examining 100 + year time scale changes in temperature and assumed forcing. In contrast to Lewis and Curry, we use a time-dependent model, which allows us to examine features such as the acceleration of deep-ocean (0–2000 m) warming in recent decades (Cheng et al. 2019). The other difference is that we focus on the most recent 52 years (1970–2021) during which radiative forcing from greenhouse gas increases has been the largest and when observed deep-ocean temperature changes are the largest and have the least measurement error. This hopefully maximizes the signal-to-noise of the EffCS estimation, keeping in mind that the time period cannot be too short otherwise natural interannual climate variations can corrupt the diagnoses (e.g., Gregory et al. 2020). While the largest volcanic eruption in modern history occurred during this period (Mt. Pinatubo in 1991, e.g. Robock 2000), it was positioned near the middle of the period, hopefully reducing its impact on the computed temperature trends and associated uncertainties in volcanic radiative forcing (Gregory et al. 2020).

While the simplicity of the model allows simulations to be carried out quickly, it is at the expense of not knowing what specific feedback processes determine EffCS. Only their net effect on the TOA radiative flux and temperature are determined. To include the effect of uncertainty in the history of radiative forcing over that period (which is quite large, mostly due to sulfate aerosol forcing uncertainty, Smith and Forster 2021), two substantially different radiative forcing histories are included. Thousands of simulations are carried out spanning the full range of observed temperature trends and potential range of model free parameters to produce frequency distributions of diagnosed EffCS for all model fits to the observational data and radiative forcing scenarios. Specifically, for each of the three model layers, an average (most likely) temperature trend is assumed, and model simulation trends ± 2 standard deviations around those means are weighted by normally distributed probabilities to arrive at probability distributions of model diagnosed EffCS. This allows a probability-weighted "best estimate" of EffCS to be computed.

2 The 1D model and radiative forcing scenarios

The 1D time-dependent model roughly follows that of Spencer and Braswell (2014), but with a simplified vertical heat transfer scheme. It computes monthly temperature departures from assumed energy equilibrium beginning in 1765 in three layers over land and ocean separately (shown schematically Fig. 2), with adjustable heat transfer coefficients between layers which act to reduce temperature departure gradients between layers. While the model could allow for land–ocean energy exchanges to be included, this will not be explored here due to a lack of accurate knowledge of changes in energy flows between land and ocean during warming. It should be kept in mind that if there is a change in the flows of energy between land and ocean through atmospheric transport, this would impact the diagnosed values of EffCS over land and ocean separately, but should have little impact on the global average EffCS. The assumed layer depths over land and ocean are also shown in Fig. 2.

The layer thicknesses represent a configuration which captures temperature changes on interannual and longer time scales. The model equation for the first layer

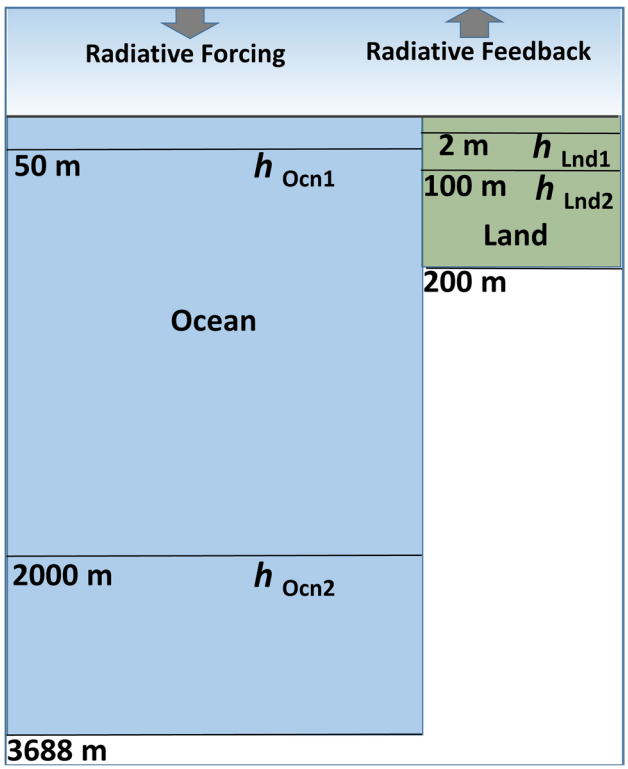

Fig. 2 Schematic of 1D forcing-feedback model, with heat transfer coefficients between layers; indicated layer depths are not to scale

temperature (T_1) departures from equilibrium ($d\Delta T_1/dt$), for either land or ocean, is

$$C_{p1}\left[d\Delta T_1/dt\right] = F(t) - \lambda T_1 - h_1\left[\Delta T_1 - \Delta T_2\right] \quad (2)$$

where C_{p1} is the bulk heat capacity of the first layer (land or ocean); F represents time-dependent radiative forcings; λ is the net feedback parameter (Forster and Taylor 2006; Forster and Gregory 2006) which is allowed to be different over land and ocean; and, h_1 is the effective vertical heat transfer coefficient (W m^{-2} K^{-1}) between the first two model layers. Note that the heat transfer coefficients have the same units as the net feedback parameter (W m^{-2} K^{-1}).

The second and third model layer temperatures are governed respectively by

$$C_{p2}\left[d\Delta T_2/dt\right] = h_1\left[\Delta T_1 - \Delta T_2\right] - h_2\left[\Delta T_2 - \Delta T_3\right] \quad (3)$$

and

$$C_{p3}\left[d\Delta T_3/dt\right] = h_2\left[\Delta T_2 - \Delta T_3\right], \quad (4)$$

where h_2 is the heat transfer coefficient between the second and third model layer. The Cp values are the product of the ocean or land volumetric heat capacity (4.186 MJ m^{-3} K^{-1} for seawater, and 2.4 MJ m^{-3} K^{-1} over land (MacDougall et al. 2010; Legutke and Voss 1999) and the thickness of the layer. The model is tested by assuming a time-constant radiative forcing of 3.7 W m^{-2} K^{-1} between 1765 and 2200, with reduced layer thicknesses and large heat transfer coefficients, to ensure all three layers asymptotically approach 1 deg. C of warming by 2200 (not shown). This ensures that the model conserves energy as intended.

Two time-varying histories of radiative forcing are used, one from CMIP5 and one from CMIP6. This is not meant to provide a full range of potential radiative forcing possibilities, but to illustrate how revised estimates of radiative forcing over the historical period can impact diagnoses of EffCS. The CMIP5 forcing is the Representative Concentration Pathways (RCP) 6.0 scenario, for which Meinshausen et al. 2011 produced the yearly time resolution estimates, here linearly interpolated to monthly assuming the annual values apply to July. While crude, the resulting impact of interpolation errors on model 52-year temperature trends will be minimal. The SSP245 effective radiative forcing values come from the tables in Annex III of IPCC (2021b), and include the AR6 best estimates up to 2019, with the SSP245 growth assumptions only included in the last three years of our model simulations (2019–2021). As such, there would be virtually no difference in the 1D model results if we used the SSP126, SSP370, or SSP585 ERF values for those final three years.

As seen in Fig. 3, these represent quite different radiative forcing scenarios, especially in terms of the rate of growth during the period we will be addressing temperature trends (1970–2021). To obtain a yearly time series from the SSP245, best estimates of effective radiative forcing (ERF, dots in Fig. 3) piecewise-linear time-dependent adjustments to the yearly resolution RCP6 radiative forcing history are used to produce a yearly resolution SSP245 that includes the major volcanic eruptions seen in RCP6, and approximately matches the benchmark years in which the SSP245 values were tabulated.

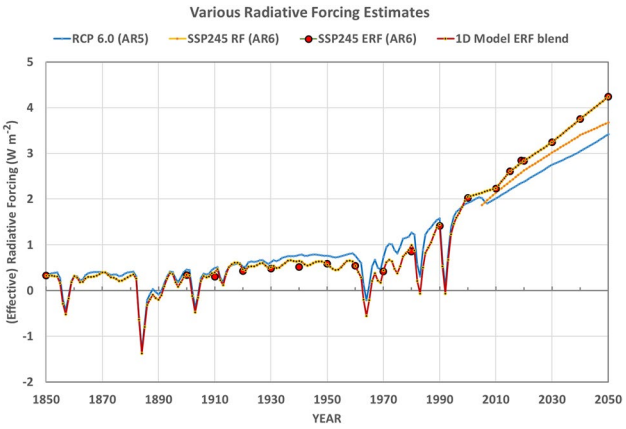

Fig. 3 Radiative forcing scenarios used in the study

3 Validation datasets

The ocean surface temperature trends (1970–2021), to which the 1D model simulations are matched, come from three datasets: HadCRUT5 (Morice et al. 2020), NOAA Global Temp (Menne et al. 2018); and Berkeley (Rohde and Hausfather 2020). For land surface air temperature, four datasets were used: the three just mentioned, and GISTEMP v4 (Lenssen et al. 2019). To qualify as a match to observations, the ocean model's first layer temperature trend needs to match any trend within the range represented by the average of the four observational land surface temperature datasets (+0.2788 deg. C per decade) ± two standard deviations (±0.0436 deg. C per decade), while the sea surface temperature trends must fall within the range represented by the average of the three SST datasets (+0.143 deg. C per decade) ± 0.0509 deg. C per decade. Each model trend falling in that range is then weighted with normally distributed probabilities over the 2-sigma range, 1.0 at the mean trend value and 0.135 at the ±2σ extremes.

The observed surface temperature trends during 1970–2021 are on the low side of those produced by 36 CMIP6 models (Fig. 4), especially for the ocean. The land/ocean warming ratio (WR) based upon these trends averages 1.45 across all of the models, compared to 1.95 from

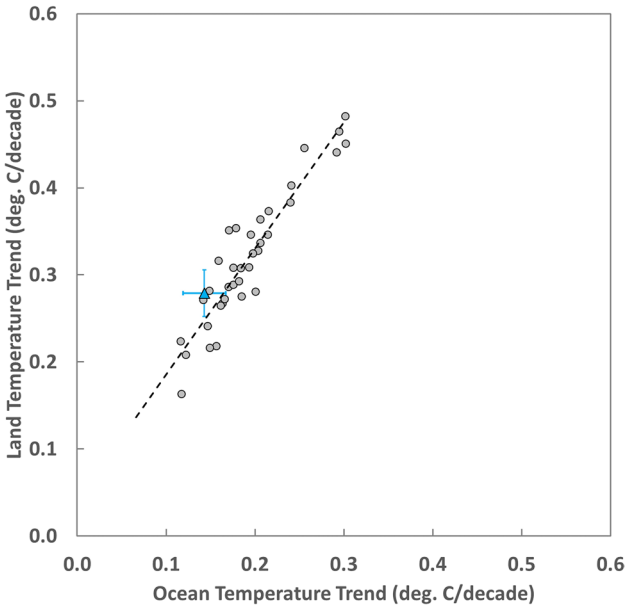

Fig. 4 Surface temperature trends over global average land versus ocean during 1970–2021 for 36 CMIP6 models (dots) forced with the SSP245 emissions scenario versus the observational datasets (and their ranges) used here (triangle)

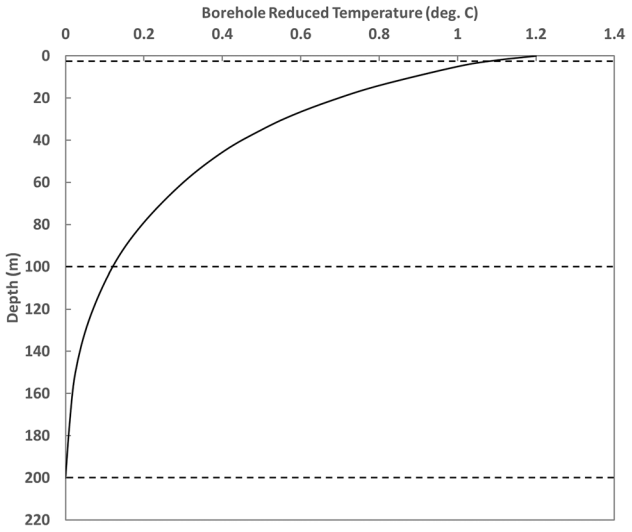

Fig. 5 Land borehole retrieved temperature change profile over the last 100–200 years adapted from Harris and Chapman (2001), used here to match 1D model inter-layer warming ratios, dashed lines indicating layer boundaries

the average of the observational datasets. Wallace and Joshi (2018) determined that this discrepancy was mostly due to incomplete spatial sampling of land areas by the thermometer network.

The ocean 0–2000 m temperature trends of Cheng et al. (2017, +0.143 deg. C/decade) must be matched by the model to within ± 20% of that value which covers the full range of trends in the datasets of Ishii et al. (2017), Dominigues et al. (2008), and Levitus et al. (2012). Similar to the surface layer matching described above, the ± 20% is assumed to be ± two standard deviations about the mean, with all 1D model trends falling in that range being weighted by normally distributed probabilities between 1.0 at the Cheng trend value and 0.135 at the ± 2σ trend values.

The bottom ocean layer in the model (2000 m to ocean bottom) is required to warm a total of 0.012 (± 40%) deg. C from 1990 to 2021 to agree with the Cheng et al. (2017, based upon Purkey and Johnson 2010 and von Schuckmann et al. 2020) estimate of 30 ZJ of warming below 2,000 m depth since 1990. This produces a 1970–2021 target trend of + 0.0031 deg. C/decade, with ± 40% assumed to cover the ± 2σ range of trend uncertainty.

Knowledge of sub-surface warming over land is not as well established as it is for the ocean. To provide a target for model sub-surface warming, the Northern Hemisphere mid-latitude borehole study of Harris and Chapman (2001) was used. In that work, a retrieved profile of sub-surface temperature changes over the last 100–200 years showed warming extending as deep as 200 m, with an approximation to their model fit to observations reproduced in Fig. 5.

We do not use the actual values of warming from Fig. 5, but instead assume the shape of land warming profile with depth during 1970–2021 is the same. Their retrieved profile of warming showed that the surface (and thus our first model layer of depth 2 m of soil) has warmed at about 2.5 times the rate of the uppermost 100 m, while the ratio of surface warming to 100–200 m layer warming is about 30. The target temperature trends using the average of the four land datasets is then 0.2788 deg. C/decade for the top land layer, with a 2σ range of 0.0436 deg. C/decade coming from the measured standard deviation of those four dataset trends. Using the warming ratio of 2.5 and 30 for the second and third land layers relative to the top layer, respectively, gives trend targets for those two layers, and we assume a 2σ range of ± 40% for those target trend values.

4 1D model experiments

The model is initialized in 1765, and each of the model's three free parameters (λ and two inter-layer heat transfer coefficients) was changed independently with closely spaced values covering a range sufficient to encompass all 1D model temperature trend matches with observations (1970–2021), including their ± 2σ ranges. These ranges were λ = 0.4 to 4.4 in intervals of 0.01 (covering EffCS = 0.84 – 9.25 deg. C); h_1 = 0.01 to 0.51 in intervals of 0.004 and h_2 = 0.001 to 0.051 in intervals of 0.0004 for land; and h_1 = 0.2 to 5.2 in

intervals of 0.04 and $h_2 = 0.1$ to 2.6 in intervals of 0.02 for ocean (all in W m-2 K-1).

The resulting frequency distributions of diagnosed EffCS values are shown in Fig. 6 for land and ocean separately, and for the two radiative forcing scenarios, separately.

The statistics from these distributions are shown in Table 1, including the ± 34% EffCS ranges, the distribution-weighted averages, and the "most probable" (50% cumulative distribution point) values.

The fits of the 1D model 0–2000 m ocean layer (distribution-weighted average of all 1D model solutions) to the Cheng et al. (2017) dataset (Fig. 7) suggest more acceleration of ocean heat storage since approximately 1990 with the SSP245 effective radiative forcing than the RCP6 radiative forcing, even though both have the same trends over the 1970–2021 period.

The 1D model results here produce somewhat higher EffCS values than those reported by Lewis and Curry (2018), which ranged from 1.5 to 1.8 deg. C for the global average compared to 1.86 deg. C here using the SSP245 effective radiative forcing estimates. This difference is not surprising given the difference in time periods addressed, and our inclusion of deep-ocean (below 2000 m) and deep-land heat storage, both of which will act to increase the estimate of EffCS. Also, the strong dependence of EffCS on which radiative forcing history is used is likely to also affect the results.

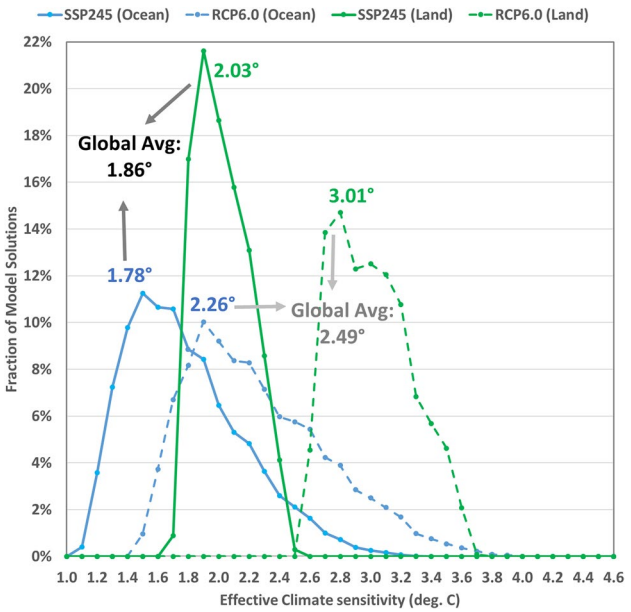

Fig. 6 Frequency distributions of 1D model-diagnosed EffCS for land and ocean, separately, and for two radiative forcing scenarios, RCP6 and SSP245. Indicated averages are for the full distributions; "most probable" (50% cumulative distribution point) values are somewhat lower (see Table 1)

Table 1 1D model EffCS distribution statistics (deg. C) from the distributions shown in Fig. 6

	± 34% range	Distribution-weighted average	Most probable
SSP245 Ocean	1.35° – 2.13°	1.78°	1.61°
SSP245 Land	1.79° – 2.18°	2.03°	1.95°
SSP245 Global	1.48° – 2.15°	1.86°	1.71°
RCP6 Ocean	1.76° – 2.70°	2.26°	2.14°
RCP6 Land	2.68° – 3.25°	3.01°	2.94°
RCP6 Global	2.04° – 2.87°	2.49°	2.38°

Note that the newer SSP245 effective radiative forcing estimates produce considerably lower EffCS values than do the RCP6 estimates, with a probability distribution-weighted average of 2.03 deg. C for land and 1.78 deg. C for ocean, for a global average of 1.86 deg. C (range 1.48 to 2.15). The RCP6 radiative forcing scenario produces 3.01 deg. C for land, 2.26 deg. C for ocean, with a global average EffCS of 2.49 deg. C (range 2.04 to 2.87). The "most probable" (50% cumulative distribution point) EffCS values in Table 1 are somewhat lower than the distribution-weighted average values

Note the ranges of diagnosed EffCS in Fig. 6 and Table 1 are rather large, a reflection of the uncertainties in the variety of observational dataset temperature trends over land and ocean, but also the changing estimates of historical radiative forcing between the CMIP5 and CMIP6 model assessments. The EffCS diagnosed from SSP245 here (1.86 deg. C) is qualitatively consistent with the somewhat lower observed surface temperature trend in Fig. 1 compared to the CMIP6 models, keeping in mind that deep-ocean (and land) heat storage differences with the CMIP6 models will also affect the comparison. Only 2 of the 36 CMIP6 models in Figs. 1 and 4 have ECS lower than 2.0 deg. C, INM-CM4-8 and INM-CM5-0 (Meehl et al. 2020)

The 1D model-diagnosed EffCS and the average observed surface temperature trends from the four land and three ocean datasets can be compared with the corresponding metrics from 36 CMIP6 models (Fig. 8). It can be seen that the closest match of the 1D model result is to the two Russian models (INM-CM4 and INM-CM5).

This result supports a variety of other studies that have noted observed warming trends in recent decades are generally lower than what are produced by most CMIP6 models (Scafetta 2022 and references therein). Due to short-term internal climate variability, several models in Fig. 8 are seen to produce lower surface temperature trends during 1970–2021 than in observations, but the 1D model-diagnosed best-estimate of EffCS in Fig. 8 is not inconsistent with the observed surface trend. Again, it should be kept in mind that the 1D model EffCS is based upon the 52-year (1970–2021) historical period, whereas the CMIP6 model EffCS values were diagnosed from the first 150 years of 4XCO2 model experiments where the evolving model TOA radiative imbalance is regressed against surface warming, and extrapolating that relationship to zero TOA radiative imbalance.

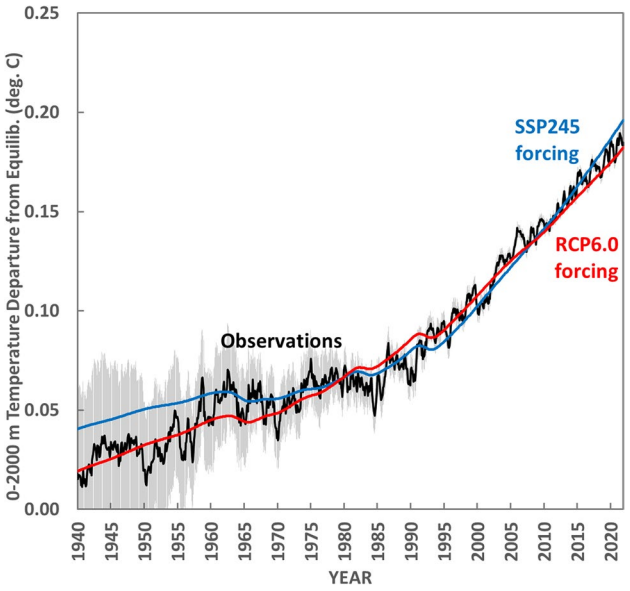

Fig. 7 Fit of the 1D model distribution-weighted average temperature solutions to the Cheng et al. (2017) 0–2000 m temperature observations (black line, with uncertainty bars) when using SSP245 (blue) or RCP6.0 (red) radiative forcing histories, matching the linear trends during 1970–2021; the vertical scale applies to the SSP245 simulation, while the other two time series have been vertically offset for alignment

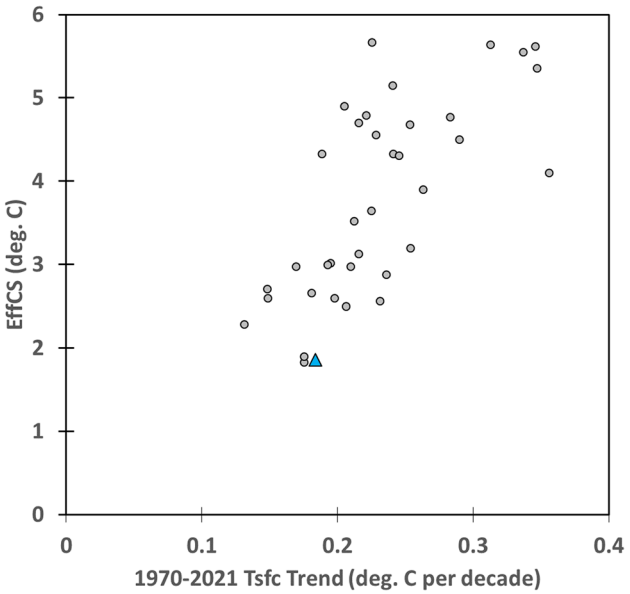

Fig. 8 CMIP6 model EffCS values as compiled by Zelinka et al. (2020) and other sources versus the 1970–2021 global average surface temperature trends from those models (dots), and the 1D model result from the present study (triangle)

5 Summary and discussion

We attempt to answer the question, What effective climate sensitivity is consistent with the observed rates of land and deep-ocean warming over the last 50 + years? The observed rate of surface warming during that time is less than produced by 80% of 36 CMIP6 climate models, and the CMIP6 models still have documented problems with energy conservation and produce future warming rates that vary by a factor of three. To address this question, a 1D time-dependent model of global monthly average temperature departures from energy equilibrium was forced with the newer SSP245 and older RCP6 radiative forcing scenarios. The primary model adjustable parameters are the net radiative feedback parameter (which determines the effective climate sensitivity) and two heat transfer coefficients which determine the rate of heat transfer between the three model layers, land or ocean.

When the model is run with a full range of potential values of the three free parameters, the model-produced temperature trends during 1970–2021 match the assumed range of observed trends (within 2σ error bounds), producing frequency distributions of EffCS over land and ocean, separately. Diagnosed best-estimate (probability distribution-weighted) EffCS is higher over land than over ocean, consistent with greater observed warming trends there. Global average EffCS is 1.86 deg. C. for the SSP245 ERF scenario, and 2.49 deg. C for the RCP6 scenario. These are near the lower end of the most recent climate sensitivity estimates from IPCC (2021a) of 2.5 to 4.0 deg. C, although the possibility of EffCS increasing in the future cannot be addressed from the historical data analyzed here. It should also be kept in mind that the 1D EffCS diagnosis is based upon observations during the historical period (1970–2021), while the CMIP6 diagnoses are from 150-year simulations forced with abrupt quadrupling of the atmospheric CO_2 concentration (4XCO2).

The 1D model results produce higher EffCS values than those reported by Lewis and Curry (2018), which ranged from 1.5 to 1.8 deg. C, despite some similarities in methodology. This difference could be from our inclusion of land heat storage to match borehole measurements and ocean heat storage below 2000 m depth, both of which will increase EffCS diagnoses. Also, we use temperature trends over the recent period (1970–2021) instead of differences over a 100 + year time scale to focus on a time period with the greatest radiative forcing change and the most accurate observational data. One large difference could be the uncertain magnitude of shortwave aerosol radiative forcing. Our results support previous observation-based studies (reviewed by Scafetta 2022) that EffCS during the historical period is in the lower range of those diagnosed

from CMIP6 models, specifically matching only the two Russian models, INM-CM4 and INM-CM5.

Our results suggest large uncertainty in diagnosing EffCS from historical land and ocean temperature data due primarily to uncertainty in real-world radiative forcing. Given that ERF from increasing CO_2 is well established, the uncertainty is likely to be in the aerosol radiative forcing over the last 50 + years.

EffCS diagnosed over land is uniformly higher than that over the ocean, which is consistent with long-term integrations from ESMs that show, irrespective of radiative forcing scenario, ~ 50% greater warming over land than ocean, for a land–ocean warming ratio (WR) of approximately 1.5 (Wallace and Joshi 2018 and references therein). For the time period addressed here (1970–2021), the observed land rate of warming is approximately twice that of the ocean, for a WR of 1.95, but Wallace and Joshi (2018) point out that the discrepancy is largely due to incomplete spatial coverage of global land masses by the thermometer record. The warming ratio of the 1D model-diagnosed EffCS is smaller than 1.5: 1.14 for the SSP245 forcing scenario and 1.33 for the RCP6 radiative forcing scenario. The 1D model presented here offers a simple yet energetically consistent method for establishing what range of effective climate sensitivities is represented by the variety of observational datasets of temperature trends to date over land and ocean, at the surface and in the sub-surface. Consistent with the fact that observed surface warming trends during 1970–2021 are weaker than in 80% of the CMIP6 models, the diagnosed EffCS is correspondingly smaller (~ 1.9 deg. C), consistent with only 2 of 36 models. The 1D model can provide a baseline for comparison to ESMs and permit evaluation of how dependent climate sensitivity estimates are to both observational datasets and to assumed radiative forcing histories. Unfortunately, for the reasons stated above, both model and observational energy-based estimates of EffCS cover a rather wide range, consistent with the conclusions of Gregory et al. (2020) that a longer period of time (e.g., into the 2030s) without a major volcanic eruption might be required to reduce the uncertainty in EffCS diagnoses.

Finally, given that global warming is first and foremost a global energy budget problem, more detailed conclusions regarding the 1D model EffCS diagnosis being lower than that diagnosed from almost all of the CMIP6 models are difficult as long as many of those models continue to have issues conserving energy (Hobbs et al. 2016; Irving et al. 2021).

Author contribution Both authors contributed to the study concept and design. Material preparation, data collection, and analysis were performed by Roy W. Spencer. The first draft of the manuscript was written by Roy W. Spencer and John R. Christy commented on all versions of the manuscript. Both authors read and approved the final manuscript.

Funding This research was funded though U.S. Department of Energy contract DE-SC0019296 and through the Alabama Office of the State Climatologist.

Data availability The 1D model, including the input datasets, input parameters, and output data, will be available at http://www.nsstc.uah.edu/data/roy.spencer.

Code availability The Fortran code used in the study will be made available at http://www.nsstc.uah.edu/data/roy.spencer.

Declarations

Ethics approval/declarations Not applicable.

Consent to participate Not applicable.

Consent for publication The authors grant TAAC sole rights to publish the submitted manuscript and we agree to the terms outlined under "Ethical Responsibilities of Authors".

Competing interests The authors declare no competing interests.

References

Burke EJ, Zhang Y, Krinner G (2020) Evaluating permafrost physics in the Coupled Model Intercomparison Project 6 (CMIP6) models and their sensitivity to climate change. Cryosphere 14:3155–3174. https://doi.org/10.5194/tc-14-3155-2020

Cheng L, Trenberth KE, Fasullo J, Boyer T, Abraham J, Zhu J (2017) Improved estimates of ocean heat content from 1960–2015. Sci Adv 3(3):e1601545 https://doi.org/10.1126/sciadv.1601545

Cheng L, Abraham J, Hausfather Z, Trenberth KE (2019) How fast are the oceans warming? Science 363(6423):128–129. https://doi.org/10.1126/science.aav7619

Cuesta-Valero FJ, García-García A, Beltrami H, Smerdon JE (2016) First assessment of continental energy storage in CMIP5 simulations. Geophys Res Lett 43(10):5326–5335. https://doi.org/10.1002/2016GL068496

Domingues CM, Church JA, White NJ, Gleckler PJ, Wijffels SE, Barker PM, Dunn JR (2008) Improved estimates of upper-ocean warming and multi-decadal sea-level rise. Nature 453:1090–1093. https://doi.org/10.1038/nature07080

Eyring V, Bony S, Meehl GA, Senior CA, Stevens B, Stouffer RJ, Taylor KE (2016) Overview of the Coupled Model Intercomparison Project Phase 6 (CMIP6) experimental design and organization. Geosci Model Dev 9:1937–1958. https://doi.org/10.5194/gmd-9-1937-2016

Forster PM, Gregory JM (2006) The climate sensitivity and its components diagnosed from Earth Radiation Budget data. J Clim 19:39–52. https://doi.org/10.1175/JCLI3611.1

Forster PM, Taylor KE (2006) Climate forcings and climate sensitivities diagnosed from coupled climate model integrations. J Clim 19:6181–6194. https://doi.org/10.1175/JCLI3974.1

Forster P, Storelvmo T, Armour K, Collins W, Dufresne J-L, Frame D, Lunt DJ, Mauritsen T, Palmer MD, Watanabe M, Wild M, Zhang H (2021) The Earth's energy budget, climate feedbacks, and climate sensitivity. In: Masson-Delmotte V, Zhai P, Pirani A, Connors SL, Péan C, Berger S, Caud N, Chen Y, Goldfarb L, Gomis MI, Huang M, Leitzell K, Lonnoy E, Matthews JBR, Maycock TK, Waterfield T, Yelekçi O, Yu R, Zhou B (eds) Climate change 2021: the physical science basis. Contribution of Working Group I to the Sixth Assessment Report of the Intergovernmental Panel on Climate Change. Cambridge University Press, Cambridge, pp 923–1054. https://doi.org/10.1017/9781009157896.009

Gregory JM, Andrews T, Ceppi P, Mauritsen T (2020) How accurately can the climate sensitivity to CO2 be estimated from historical climate change? Clim Dyn 54:129–157. https://doi.org/10.1007/s00382-019-04991-y

Harris RN, Chapman DS (2001) Mid-latitude (30°–60° N) climatic warming inferred by combining borehole temperatures with surface air temperatures. Geophys Res Lett 28:747–750. https://doi.org/10.1029/2000GL012348

Hobbs W, Palmer MD, Monselesan D (2016) An energy conservation analysis of ocean drift in the CMIP5 global coupled models. J Clim 29:1639–1653. https://doi.org/10.1175/JCLI-D-15-0477.1

IPCC (2021a) Summary for policymakers. In: Masson-Delmotte V, Zhai P, Pirani A, Connors SL, Péan C, Berger S, Caud N, Chen Y, Goldfarb L, Gomis MI, Huang M, Leitzell K, Lonnoy E, Matthews JBR, Maycock TK, Waterfield T, Yelekçi O, Yu R, Zhou B (eds) Climate change 2021: the physical science basis. Contribution of working group I to the sixth assessment report of the intergovernmental panel on climate change. Cambridge University Press, Cambridge. https://www.ipcc.ch/report/ar6/wg1/downloads/report/IPCC_AR6_WGI_SPM.pdf

IPCC (2021b) In: Dentener FJ, Hall B, Smith C (eds) Climate change 2021: the physical science basis. Contribution of Working Group I to the Sixth Assessment Report of the Intergovernmental Panel on Climate Change. Cambridge University Press, Cambridge, pp 2139–2152. https://doi.org/10.1017/9781009157896.017

Irving D, Hobbs W, Church J, Zika J (2021) A mass and energy conservation analysis of drift in the CMIP6 ensemble. J Clim 34:3157–3170. https://doi.org/10.1175/JCLI-D-20-0281.1

Ishii M, Fukuda Y, Hirahara S, Yasui S, Suzuki T, Sato K (2017) Accuracy of global upper ocean heat content estimation expected from present observational data sets. Sola 13:163–167. https://doi.org/10.2151/sola.2017-030

Legutke S, Voss R (1999) The Hamburg atmosphere-ocean coupled circulation model ECHO-G. World Data Center for Climate (WDCC) at DKRZ. https://doi.org/10.2312/WDCC/DKRZ_Report_No18

Lenssen N, Schmidt G, Hansen J, Menne M, Persin A, Ruedy R, Zyss D (2019) Improvements in the GISTEMP uncertainty model. J Geophys Res Atmos 124(12):6307–6326. https://doi.org/10.1029/2018JD029522

Levitus S, Antonov JI, Boyer TP, Baranova OK, Garcia HE, Locarnini RA, Mishonov AV, Reagan JR, Seidov D, Yarosh ES, Zweng MM (2012) World ocean heat content and thermosteric sea level change (0–2000 m), 1955–2010. Geophys Res Lett 39:1–5. https://doi.org/10.1029/2012GL051106

Lewis N, Curry J (2018) The impact of recent forcing and ocean heat uptake data on estimates of climate sensitivity. J Clim 31:6051–6071. https://doi.org/10.1175/JCLI-D-17-0667.1

MacDougall AH, González-Rouco JF, Stevens MB, Beltrami H (2008) Quantification of subsurface heat storage in a GCM simulation. Geophys Res Lett 35:L13702. https://doi.org/10.1029/2008GL034639

MacDougall AH, Beltrami H, González-Rouco JF, Stevens MB, Bourlon E (2010) Comparison of observed and general circulation model derived continental subsurface heat flux in the Northern Hemisphere. J Geophys Res-Atmos 115:D12109. https://doi.org/10.1029/2009JD013170

Meehl GA, Hu A, Arblaster JM, Fasullo J, Trenberth KE (2013) Externally forced and internally generated decadal climate variability associated with the Interdecadal Pacific Oscillation. J Clim 26:7298–7310. https://doi.org/10.1175/JCLI-D-12-00548.1

Meehl GA, Senior CA, Eyring V, Flato G, Lamarque J-F, Stouffer RJ, Taylor KE, Schlund M (2020) Context for interpreting equilibrium climate sensitivity and transient climate response from the CMIP6 Earth system models. Sci Adv 6:26. https://doi.org/10.1126/sciadv.aba1981

Meinshausen M, Smith SJ, Calvin KV, Daniel JS, Kainuma MLT, Lamarque J-F, Matsumoto K, Montzka SA, Raper SCB, Riahi K, Thomson AM, Velders GJM, van Vuuren D (2011) The RCP greenhouse gas concentrations and their extension from 1765 to 2300. Clim Change 109:213–241. https://doi.org/10.1007/s10584-011-0156-z

Menne MJ, Williams CN, Gleason BE, Rennie JJ, Lawrimore JH (2018) The Global Historical Climatology Network Monthly Temperature Dataset, Version 4. J Clim 31:24. https://doi.org/10.1175/JCLI-D-18-0094.1

Morice CP, Kennedy JJ, Rayner NA, Winn JP, Hogan E, Killick RE, Dunn RJH, Osborn TJ, Jones PD, Simpson IR (2020) An updated assessment of near-surface temperature change from 1850: the HadCRUT5 data set. J Geophys Res-Atmos 126:3. https://doi.org/10.1029/2019JD032361

National Research Council (1979) Carbon dioxide and climate: a scientific assessment. The National Academies Press, Washington, DC. https://doi.org/10.17226/12181

National Research Council (2006) Surface temperature reconstructions for the last 2,000 years. National Academies Press, Washington, DC, 160 pp. https://doi.org/10.17226/11676

Purkey S, Johnson G (2010) Warming of global abyssal and deep southern ocean waters between the 1990s and 2000s: contributions to global heat and sea level rise budgets. J Clim 23:6336–6351. https://doi.org/10.1175/2010JCLI3682.1

Robock A (2000) Volcanic eruptions and climate. Rev Geophys 38(2):191–219. https://doi.org/10.1029/1998RG000054

Rohde RA (2020) Hausfather Z (2020) The Berkeley Earth land/ocean temperature record. Earth Sys Sci Data 12:3469–3479. https://doi.org/10.5194/essd-12-3469-2020

Scafetta N (2022) Advanced testing of low, medium and high ECS CMIP6 GCM simulations versus ERA5-T2m. Geophys Res Lett 49:1–15. https://doi.org/10.1029/2022GL097716

Smith J, Forster PM (2021) Suppressed late-20th century warming in CMIP6 models explained by forcing and feedbacks. Geophys Res Lett 48:19. https://doi.org/10.1029/2021GL094948

Spencer RW, Braswell WD (2011) On the misdiagnosis of surface temperature feedbacks from variations in Earth's radiant energy balance. Rem Sens 3:1603–1613. https://doi.org/10.3390/rs3081603

Spencer RW, Braswell WD (2014) The role of ENSO in global ocean temperature changes during 1955–2011 simulated with a 1D climate model. Asia-Pac J Atmos Sci 50(2):229–237. https://doi.org/10.1007/s13143-014-0011-z

von Schuckmann K, Cheng L, Palmer MD, Hansen J, Tassone C, Aich V, Adusumilli S, Beltrami H, Boyer T, Cuesta-Valero FJ, Desbruyères D, Domingues C, García-García A, Gentine P, Gilson J, Gorfer M, Haimberger L, Ishii M, Johnson GC, Killick R, King BA, Kirchengast G, Kolodziejczyk N, Lyman J, Marzeion B, Mayer M, Monier M, Monselesan DP, Purkey S, Roemmich D, Schweiger A, Seneviratne SI, Shepherd A, Slater DA, Steiner AK, Straneo F, Timmermans M-L, Wijffels SE (2020) Heat stored in the Earth system: where does the energy go? Earth Sys Sci Data 12:2013–2041. https://doi.org/10.5194/essd-12-2013-2020

Wallace CJ, Joshi M (2018) Comparison of land–ocean warming ratios in updated observed records and CMIP5 climate models. Environ Res Lett 13:114011. https://doi.org/10.1088/1748-9326/aae46f

Zelinka M, Myers T, Mccoy D, Po-Chedley S, Caldwell P, Ceppi P, Klein S, Taylor K (2020) Causes of higher climate sensitivity in CMIP6 models. Geophys Res Lett 47:1–12. https://doi.org/10.1029/2019GL085782